THE JOURNAL OF PHYSICAL CHEMISTRY B

Article

Cite This: J. Phys. Chem. B 2019, 123, 8970−8975

pubs.acs.org/JPCB

Explaining Spectral Asymmetries and Excitonic Characters of the Core Pigment Pairs in the Bacterial Reaction Center Using a Screened Range-Separated Hybrid Functional

Huseyin Aksu,[†] Alexander Schubert,[†,‡] Eitan Geva,[‡] and Barry D. Dunietz*[,†]

[†]Department of Chemistry and Biochemistry, Kent State University, Kent, Ohio 44242, United States

[‡]Department of Chemistry, University of Michigan, Ann Arbor, Michigan 48109, United States

Supporting Information

ABSTRACT: Spectral peaks of the special pair (P) and adjacent pigments in the bacterial reaction center (BRC) are investigated computationally. We employ a novel framework based on a polarization-consistent treatment of the dielectric environment, combining the polarizable continuum model (PCM) with time-dependent screened range-separated hybrid (SRSH) density functional theory. Our calculations quantitatively reproduce recently measured spectral peak splits between P excitonic states and spectral asymmetries within the pairs of excited states of the adjacent bacteriochlorophyll *a* (BChl) and bacteriopheophytin *a* (BPhe) pigments. For the special pair, a splitting energy between the absorptive state and a blue-shifted semidark state of 0.07 eV is found in close agreement with the measured value. The spectral asymmetries within the pseudosymmetric pairs of BChl and BPhe pigments are interpreted to result from locally different effective dielectric environments in the A and the B branch, where the latter are exposed to a lesser polarizing environment. We base our analysis on X-ray-resolved structures and where the effect of neighboring pigments on the electronic structure is addressed through an effective dielectric environment. We show that the spectral trends are only reproduced using a polarization-consistent framework based on a screened range-separated hybrid functional, whereas B3LYP-PCM energies fail to provide the correct trends.

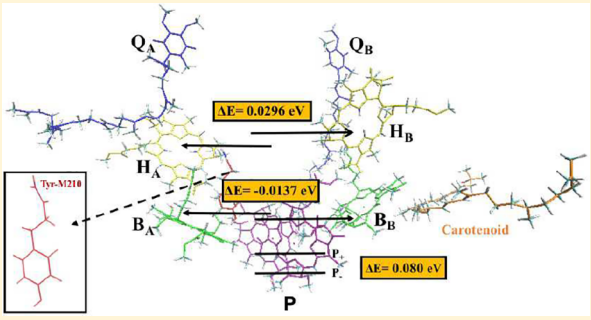

INTRODUCTION

Over the past two decades, our understanding of photosynthesis has significantly improved through advances in the structural resolution and spectral characterization.[1] Natural photosystems (PSs) are made of pigments arranged in two pseudosymmetric branches embedded within a protein matrix. The protein matrix associated with the two pseudosymmetric branches of PSs is believed to lead to distinct dielectric environments and to geometrical differences. As early as 1994, Steffen and Boxer[2] pointed at the dielectric asymmetry experienced by the branches as responsible for the striking difference of their contribution to the photosynthetic process.[3] According to this picture, pigments in branch A are subjected to less shielding (resulting in a larger effective dielectric constant) than that experienced by the pigments of branch B, which are affected by the nearby hydrophobic carotenoid. Consequently, the charge transfer photosynthetic process is understood to be driven by branch A pigments.[3]

In spite of the large-scale efforts and important advances, the complexity of the photosystems (PSs) continues to hinder a complete molecular level understanding of their structure−function relationships. In particular, resolving at the molecular level the role of dielectric asymmetry in the mechanism of photosynthesis[4−8] remains an important objective. Such asymmetry that is understood to affect the photosynthetic charge transfer steps may also affect the preceding exciton generation and transport. Here we focus on the photogenerated excited states of the core pigments of the bacterial reaction center (BRC) found in oxygenic organisms, where we account for the effect of the environment on their electronic structure.

The BRC pseudosymmetric core consists of the special pair (P), i.e., a bacteriochlorophyll *a* (BChl) dimer unit at the origin of the two branches as well as two additional BChl, denoted B_A and B_B, and two bacteriopheophytin *a* (BPhe), denoted H_A and H_B (subscripts indicate the branch). See representation of the BRC and the core pigments in Figure 1. The three pigment pairs are the main contributors to the Q_y absorption bands exhibited by the BRC. There have been several computational studies targeting BRC systems[4,6,7,9] including studies focusing on the Q_y spectra[10,11] of the core pigments as the BChl monomer[12] and BChl dimers.[13−15] However, open questions regarding these bands remain. For example, a proper characterization of the blue-shifted P state is

Received: August 10, 2019
Revised: September 26, 2019
Published: October 14, 2019

DOI: 10.1021/acs.jpcb.9b07646
J. Phys. Chem. B 2019, 123, 8970−8975

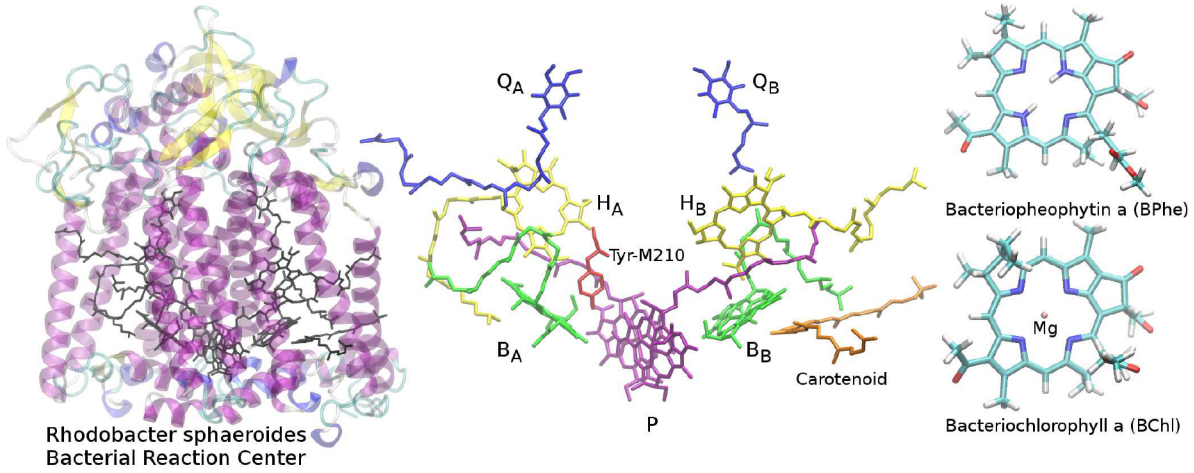

Figure 1. Representation of the BRC of *Rhodobacter sphaeroides* based on X-ray study[23] is shown to the left. The core pigment units are the P, and the pairs of BChl, and BPhe, shown in the central part along with representation of their neighboring pigments that form the distinct effective dielectric for the two branches. The carotenoid adjacent to B_B and a polarizing Tyr-M210 affecting B_A lead to a more shielded B_B pigment than the shielding affecting B_A pigment. A pair of quinones (Q) adjacent to the BPhe pigments are also shown. In the right part we illustrate the BChl and BPhe molecular models used in the calculations where phytyl tails are replaced by hydrogens.

required to investigate its role in capturing the excitation energy as hypothesized by earlier studies.[7,16] The actual spectral splitting in the P bands is difficult to resolve since the blue-shifted state is a dark state that eludes spectral studies.[16−21] Other spectral trends related to the BChl pair and the BPhe pair are also challenging full understanding, where the B_A state is blue-shifted over that of B_B, whereas a red-shift is indicated for the H_A state over the H_B one.[16−21]

In this study, we investigate the spectral properties of BRC in the purple bacterium *Rhodobacter sphaeroides* and compare calculated pigments electronic states to peaks in linear absorption and two-dimensional electronic spectra of *Rhodobacter capsulatus*, reported by Niedringhaus et al.[16] We associate spectral trends of the pigment pairs to the pigments' electronic structure and explain the relationships of the spectra with structural and environmental asymmetries. Such understanding is crucial to develop well-parametrized models to study energy and charge transfer processes involving these pigments.[22]

In particular, we address the following experimental observations reported in ref 16 (additional measurements are discussed below for the sake of completeness): (i) The special pair spectral splitting of 0.081 eV between the lowest absorptive electronically excited dimer state (P_-^*) and a blue-shifted semidark state (P_+^*); (ii) the two pseudosymmetric BChl and BPhe pairs show opposite spectral shifts: while the absorption energy of B_A is blue-shifted by 0.014 eV with respect to B_B, the H_A energy is red-shifted by 0.030 eV with respect to H_B. Below we report our analysis of the measured spectral features of the core pigments in BRC showing *relative shifts* in the BChl and BPhe pigment peaks due to A and B branch asymmetries and *excitonic splitting* in the P.

METHOD

While a comprehensive treatment of complex molecular systems like the PSs is becoming affordable through recent developments as of subsystem DFT methods[24−26] with excited-state calculations,[24,27,28] which were followed by applications to study PSs,[29,30] here we employ a recently developed polarization-consistent framework[31] combining the polarizable continuum model (PCM) with time-dependent density functional theory (TDDFT) by using a screened range-separated hybrid functional (SRSH). The SRSH-PCM method is both cost-effective and accurate for obtaining ground- and excited-state properties of a molecular system affected by a polarizing condensed phase environment in single molecule calculations. In the SRSH-PCM approach[31] the same dielectric constant that is invoked in the self-consistent reaction-field iterations implementing the PCM is used in setting the SRSH functional parameters to screen the long-range (LR) Coulomb interactions. Thus, the SRSH-PCM frontier orbitals reproduce electron removal or addition energies measured in the condensed phase,[31] and when used in TDDFT calculations,[32] lead to excitation energies that agree with measured solvated charge transfer (CT) state energies. More recently, SRSH-PCM was used to explain the spectral features of pentacoordinated BChl and chlorophyll *a*, which deviate from the Gouterman model, by resolving the controversial assignment of the blue-shifted peak to either electronic state or vibronic progression.[33] These successful studies are especially promising in light of well-known caveats of DFT calculations.

The SRSH-PCM follows the generalized exchange-correlation functional formulation where the energy expression is

$$E_{XC}^{SRSH} = \alpha E_{F_X}^{SR} + (1-\alpha)E_{PBE_X}^{SR} + (\alpha+\beta)E_{F_X}^{LR} + (1-\alpha-\beta)E_{PBE_X}^{LR} + E_{PBE_C} \quad (1)$$

Here, the subscripts "X" and "C" denote exchange and correlation, the subscripts "F" and "PBE" denote Fock and PBE exchange, and the superscripts "SR" and "LR" denote short range and long range. In this SRSH exchange-correlation expression, α determines the fraction of Fock exchange in the short range, $\alpha+\beta$ determines the fraction of Fock exchange in the long range and is set to $1/\epsilon$, the inverse of the dielectric constant employed in the PCM. The SRSH-PCM functional sidesteps the well-known limitation due to numerical instability in PCM-based tuning of the range separation parameter,[34,35] where an alternative tuning can be pursued.[31]

To clarify, all the excited state energies reported below are calculated by using the polarization-consistent SRSH-PCM

DOI: 10.1021/acs.jpcb.9b07646
J. Phys. Chem. B 2019, 123, 8970−8975

framework[31,32] employing the ωPBE-h functional and 6-31G** basis set at the state specific[36,37] nonequilbrium PCM level[38] with a static dielectric constant that is varied for the analysis, and the optical dielectric constant of water (ϵ_∞ = 1.78) was used in all calculations as we assume that the organic molecular screening environment is associated with a similar optical dielectric effect. (The SRSH functional parameters at various dielectric constants are provided in the Supporting Information, Table S1.) The same level of TDDFT theory was recently benchmarked successfully in studying solvated CT state energies.[32] Geometries are obtained by optimizing the pigment structures by using the X-ray structures as the initial geometry[23] (these coordinates are provided in the Supporting Information) at the dispersion-corrected ωB97X-D functional with the 6-31G* basis set level within the PCM employing the same dielectric constant ϵ as used in the subsequent TD-DFT calculations. For simplicity, phytyl tails are removed as these are indicated to bear only a minimal effect on excitation energies.[12] The calculations were implemented by using the Q-Chem software package.[39]

In Figure 1 we illustrate the core pigment units that are at the base of the two branches within the BRC. We also indicate the distinct molecular environment of the branches including the hydrophobic carotene that shields the B_B pigment and the polarizing Tyr-M210 affecting the branch A pigments (see the middle panel of Figure 1).

RESULTS AND DISCUSSION

We begin our analysis by considering the spectral splitting of the P excitonic states. There appears to be controversy on the role of the blue-shifted semidark P_+^* state in exciton transfer and charge separation and whether it is blue-shifted sufficiently to overlap in energy with the adjacent B pigments spectral bands. The recent 2D electronic spectra (2DES) of BRC[16] place the P semidark state, P_+^*, at 0.08 eV above the absorptive P state, P_-^*. Other spectral studies based on hole-burning,[17,18,20,40] linear dichroism[41] and pump−probe experiments[19] find a larger splitting energy of about 0.1 eV.

In Figure 2, we follow the spectral splitting upon change of the dielectric constant. Note that excitation energies appear to overestimate the measured values by 0.2−0.3 eV, while the energy splittings or shifts (discussed below) are well reproduced. Such an overestimation tendency was reported[42] and may reflect structural constraints due to the molecular environment that appear to not affect the spectral splitting or shifting energies. The state excitation energies and oscillator strengths are listed in Table S2. Importantly, our calculations are consistent with the 2DES splitting energy of 0.08 eV[16] with a dark-blue-shifted state. Within the relevant range of dielectric constants the calculated splitting energy maximizes with 0.07 eV at the range of 1.7−1.8, whereas it drops significantly with constants that are below 1.2 and above 2.0.

At the lower dielectric constant up to 1.7, the S1 and S2 states correspond each mainly to the HOMO-to-LUMO transition and HOMO-to-LUMO+1 transition, respectively. However, further increase of the dielectric constant leads to state crossing with the intrapair CT states, where we find an increase of the CT character in both states. The splitting collapses above a dielectric of 2.1, where the CT states are stabilized to become the lowest states of the special pair. We provide further analysis of the CT states within the P and to the adjacent pigment in a future report. In Table S2 we follow the oscillator strengths (OSs) of the excitonic P states. The

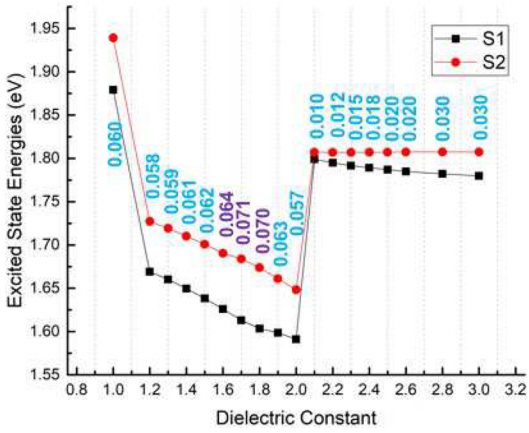

Figure 2. P excited state energies at various dielectric constants calculated by using SRSH-PCM. The calculated spectral splitting of 0.07 eV with dielectric constants of 1.7−1.8 is in reasonable agreement with the measured spectral splitting of 0.08 eV based on the 2DES reported in ref 16. The excitation energies and oscillator strengths at the different dielectric constants are tabulated in Table S2.

ratio of the two OSs of about a factor of 3, with S1 being the brighter state, with constants of 1.6−1.9, is in good agreement with the measured spectra.[16]

We now address the excited states associated with the pigment pairs adjacent to P. The absorption energy of B_A is found to be blue-shifted with respect to B_B, whereas H_A is found to be red-shifted with respect to H_B.[16,43] Therefore, the BChl energy is expected to increase and that of the BPhe to decrease with the increase of the dielectric constant. (This is required by following the understanding that branch A pigments are affected by a higher dielectric constant than that affecting the branch B pigments and assuming that geometrical differences are sufficiently small.) Figure 3 shows that in the case of B3LYP both pigment excitation energies increase with the dielectric constant. On the other hand, the

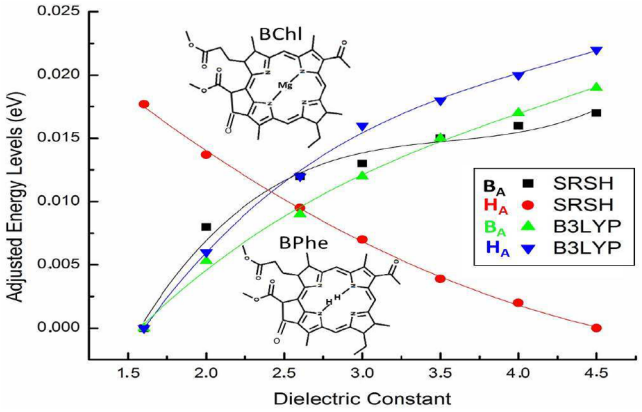

Figure 3. Dependence of the excited state energies of BChl and BPhe on the dielectric constant calculated by using SRSH-PCM and B3LYP-PCM at the ωB97X-D optimized geometries. Here we use the geometries corresponding to B_A and H_A, where similar trends are indicated for branch B structures. The expected trends where the BChl energy is blue-shifted and that of the BPhe is red-shifted with the increase of the dielectric constant are found for the SRSH energies but not with B3LYP values. The corresponding excited state energies are tabulated in Table S3.

DOI: 10.1021/acs.jpcb.9b07646
J. Phys. Chem. B 2019, 123, 8970−8975

SRSH-PCM calculated energies correctly reproduce these opposite spectral trends. The figure shows excitation energies of branch A pigments. (We confirm the same trends when branch B geometries are used.)

The opposite trends due to the dielectric in BChl versus that in BPhe are found to result from the Mg(II) ion that is ligated in BChl but is not present in BPhe. This is confirmed by following the excitation energies as affected by the dielectric constant upon removing (adding) the ion from the BChl (BPhe) pigment. Indeed, both trends are reversed upon such changes (see Table 1). Our finding on the role of the Mg(II) ion ligation of the BChl pigments on the excitation energies is in agreement with earlier studies.[44] The analysis above was performed using ωB97X-D-optimized structures. Spectral trends based on B3LYP-optimized structures are provided in Table S5. Here both the SRSH and B3LYP excitation energies fail to present the correct trend highlighting the importance of using the dispersion-corrected functionals in the geometry optimizations. Therefore, in the following only SRSH energies for pigment geometries obtained with ωB97X-D are considered.

Table 1. Excitation Energies (eV) of B'_A and B'_B (Where the Mg(II) Ion Is Removed) and H'_A and H'_B (Where a Ligated Mg(II) Ion Is Added)[a]

ϵ	B'_A	B'_B	H'_A	H'_B
2.0	1.9873	1.9762	1.9129	1.9364
3.5	1.9865	1.9756	1.9169	1.9406
4.0	1.9862	1.9754	1.9176	1.9423
4.5	1.9848	1.9738	1.9226	1.9526

[a]Geometries have been reoptimized.

The excited state energies of the two pairs of pigments are shown over the relevant range of low dielectric constants in Figure 4. Energy differences, where the calculated excitation energies are fitted to a fourth-order polynomial, are shown by the solid lines; the calculated energies are shown by squares and circles for the branch A and B pigments, respectively. Spectral differences based on energies obtained with the same dielectric constant (values shown in vertical font) capture approximately 2/3 of the measured energy difference. The remaining energy difference may result from the dielectric asymmetry where a larger dielectric is assigned to branch A pigment.

Several dielectric constants pairing that result with the measured differences of −0.014 and 0.030 eV for the BChl and BPhe pairs are indicated by the slanted lines with the extent of dielectric constant asymmetry provided in the adjacent box. For example, a dielectric constant assigned to B_B of 2.7 is associated with a 4.7 for B_A, and a dielectric constant for H_B of 2.4 leads to a 4.0 constant for H_A. For both types of pigments pairs the indicated dielectric asymmetry appears to rise as the dielectric constants increase, while the slopes of the energies appear to saturate with the increase of the dielectric. (Larger structural differences have been indicated for the BChl pigment pair in an earlier X-ray resolved structure.[45] In such case a smaller dielectric asymmetry is required to reproduce the spectral shift.[43])

We point out that the molecular environment of B_A of the phenolic −OH group of Tyr-M210[46,47] suggests smaller shielding and therefore a larger effective dielectric constant than that for the B_B which is affected by increased shielding due to a nearby nonpolar carotenoid (see Figure 1). Also represented in the figure are the two quinones, Q_A and Q_B, whose two nonpolar tails are expected to give rise to larger shielding for both BPhe pigments (compared to BChl pigments) and therefore may result in a lower dielectric constants for the BPhe pigments over those of the BChl pair.[46,47]

CONCLUSIONS

In conclusion, we analyze the electronic states associated with the pigments found at the core of the BRC by relating to their spectral signatures. Employing the recently developed polarization-consistent screening approach SRSH-PCM toward TD-DFT, the spectral splitting of the special pair and the spectral

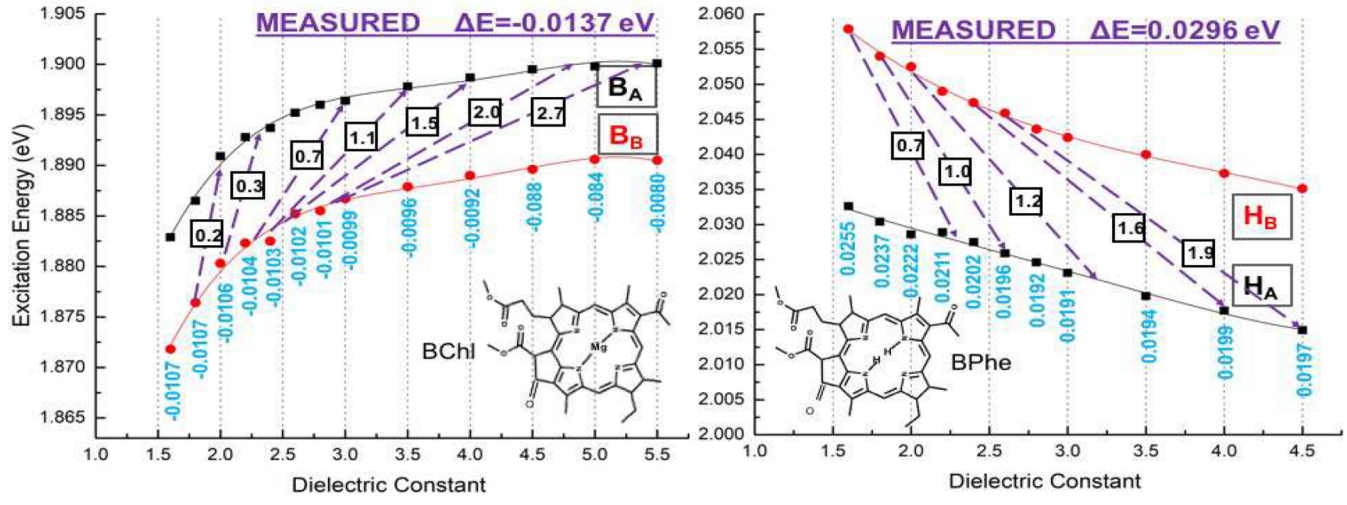

Figure 4. Excitation energies of the BChl and BPhe pigments. The branch A and B pigments energies at different dielectric constants are shown using black squares and red circles, respectively. By use of fourth-order fitted polynomials (solid lines), the spectral energies are used to estimate spectral energy branch differences due to BChl and BPhe pigments at the same dielectric constant (values listed in blue vertically aligned font), where the tilted lines indicate constants with which the energy differences are in agreement with the measured energies. The extent of dielectric constant asymmetry is indicated by the boxed numbers at the center of the tilted lines. The excited state energies are tabulated in Tables S3−S5.

DOI: 10.1021/acs.jpcb.9b07646
J. Phys. Chem. B 2019, 123, 8970−8975

shifting between the pseudosymmetric pigments of branch A and B can be traced back to the pigments effective dielectric environment and to structural differences. Our calculations support a hypothesis that the electronic states of the core pigment units (P, B_A, B_B, H_A, and H_B) are localized on the individual pigment unit, where couplings to their adjacent pigments are negligible. In the case of P we have considered the coupled dimer excitonic states. Namely, the spectral trends can be explained without introducing multimer excitonic states[48] that are extended beyond each such pigment unit and where the molecular environment affecting the photogenerated pigment-localized excited states (including the excitonic P states) is represented by an effective dielectric constant.

Here, the spectral splitting of P is well-reproduced within a range of small dielectric constants representing a strongly shielded environment. Our calculations confirm the presence of semidark state, P^*_+, blue-shifted by 0.08 eV, which is proposed to play a role as a precursor to the charge separation process.[7,16] We also address the BRC spectral asymmetry of the transitions associated with the pseudosymmetric pigment pairs adjacent to the P.[16,49] On the basis of their X-ray geometries[23,45,50] we establish relaxed structures, which are then used in SRSH-PCM calculations of excitation energies affected properly by a dielectric medium. Various combinations of dielectric constants assigned to the pigments for which the spectral differences for B_A, B_B and H_A, H_B pairs are in agreement with the measured shifts. Importantly, the polarization-consistent approach correctly reproduces the opposite-signed shifts, where the excited state energy of B_A is higher than that of B_B, while that of H_A is lower than that of H_B. These opposite trends are found to depend on the presence of a Mg(II) ion that is ligated in the BChl pigments but not in the BPhe pigments. In ongoing efforts we are investigating charge transfer states between the core pigments, which are expected to be strongly affected by the effective dielectric constant representing the environment and which may mix with the pigment site states.

■ ASSOCIATED CONTENT

Supporting Information

The Supporting Information is available free of charge on the ACS Publications website at DOI: 10.1021/acs.jpcb.9b07646.

Functional parameters, excited state properties of the different pigments at various dielectric constants, and the pigment initial structures (PDF)

■ AUTHOR INFORMATION

Corresponding Author

*E-mail: bdunietz@kent.edu.

ORCID

Huseyin Aksu: 0000-0001-9463-3236
Alexander Schubert: 0000-0002-8560-6436
Eitan Geva: 0000-0002-7935-4586
Barry D. Dunietz: 0000-0002-6982-8995

Present Address

A.S.: Institute of Physical Chemistry, Friedrich-Schiller University Jena, 07743 Jena, Germany.

Notes

The authors declare no competing financial interest.

■ ACKNOWLEDGMENTS

We are thankful to Prof. Jennifer Ogilvie for ongoing discussions and for her comments regarding the reported research. B.D.D. is grateful for support by NSF via Grant CHE-1362504. E.G. is grateful for support by NSF via Grants CHE-1464477 and CHE-1800325. A.S. is grateful for support from an ICAM fellowship, awarded by the Kent State University and University of Michigan ICAM branches. We are also grateful to generous resource allocations on the Ohio Supercomputer Center[51] and the Kent State University, College of Arts and Sciences Computing Cluster. We also thank Ms. Khadiza Begam for help in preparing the figures.

■ REFERENCES

(1) Brixner, T.; Hildner, R.; Kohler, J.; Lambert, C.; Wurthner, F. Exciton Transport in Molecular Aggregates From Natural Antennas to Synthetic Chromophore Systems. *Adv. Energy Mater.* **2017**, *7*, 1700236.

(2) Steffen, M. A.; Lao, K.; Boxer, S. G. Dielectric asymmetry in the photosynthetic reaction center. *Science* **1994**, *264*, 810−816.

(3) Saggu, M.; Fried, S. D.; Boxer, S. G. Local and Global Electric Field Asymmetry in Photosynthetic Reaction Centers. *J. Phys. Chem. B* **2019**, *123*, 1527−1536.

(4) Hasegawa, J.; Ohkawa, K.; Nakatsuji, H. Excited States of the Photosynthetic Reaction Center of Rhodopseudomonas viridis: SACCI Study. *J. Phys. Chem. B* **1998**, *102*, 10410−10419.

(5) Warshel, A.; Parson, W. W. Spectroscopic properties of photosynthetic reaction centers. 1. Theory. *J. Am. Chem. Soc.* **1987**, *109*, 6143−6152.

(6) Parson, W. W.; Warshel, A. Spectroscopic properties of photosynthetic reaction centers. 2. Application of the theory to Rhodopseudomonas viridis. *J. Am. Chem. Soc.* **1987**, *109*, 6152−6163.

(7) Jordanides, X. J.; Scholes, G. D.; Fleming, G. R. The Mechanism of Energy Transfer in the Bacterial Photosynthetic Reaction Center. *J. Phys. Chem. B* **2001**, *105*, 1652−1669.

(8) Zinth, W.; Wachtveitl, J. The First Picoseconds in Bacterial PhotosynthesisUltrafast Electron Transfer for the Efficient Conversion of Light Energy. *ChemPhysChem* **2005**, *6*, 871−880.

(9) Curutchet, C.; Mennucci, B. Quantum Chemical Studies of Light Harvesting. *Chem. Rev.* **2017**, *117*, 294−343.

(10) Wawrzyniak, P. K.; Beerepoot, M. T. P.; de Groot, H. J. M.; Buda, F. Acetyl group orientation modulates the electronic ground-state asymmetry of the special pair in purple bacterial reaction centers. *Phys. Chem. Chem. Phys.* **2011**, *13*, 10270−10279.

(11) Ikegami, T.; Ishida, T.; Fedorov, D. G.; Kitaura, K.; Inadomi, Y.; Umeda, H.; Yokokawa, M.; Sekiguchi, S. Fragment molecular orbital study of the electronic excitations in the photosynthetic reaction center of Blastochloris viridis. *J. Comput. Chem.* **2010**, *31*, 447−454.

(12) Kenny, E. P.; Kassal, I. Benchmarking Calculations of Excitonic Couplings between Bacteriochlorophylls. *J. Phys. Chem. B* **2016**, *120*, 25−32.

(13) Song, J.; Gao, F.; Liang, W. How does the nonlocal HF exchange influence the electron excitation of Bacteriochlorophyll and its assembly. *Comput. Theor. Chem.* **2011**, *965*, 53−59.

(14) Manna, A. K.; Dunietz, B. D. Communication: Charge-transfer Rate Constants in Zinc-Porphyrin-Porphyrin-derived dyads: A Fermi Golden Rule First-Principles-Based Study. *J. Chem. Phys.* **2014**, *141*, 121102.

(15) McCleese, C.; Yu, Z.; Esemoto, N. N.; Kolodziej, C.; Maiti, B.; Bhandari, S.; Dunietz, B. D.; Burda, C.; Ptaszek, M. Excitonic Interactions in Bacteriochlorin Homo-Dyads Enable Charge Transfer: A New Approach to the Artificial Photosynthetic Special Pair. *J. Phys. Chem. B* **2018**, *122*, 4131−4140.

(16) Niedringhaus, A.; Policht, V. R.; Sechrist, R.; Konar, A.; Laible, P. D.; Bocian, D. F.; Holten, D.; Kirmaier, C.; Ogilvie, J. P. Primary processes in the bacterial reaction center probed by two-dimensional

DOI: 10.1021/acs.jpcb.9b07646
J. Phys. Chem. B 2019, 123, 8970−8975

electronic spectroscopy. *Proc. Natl. Acad. Sci. U. S. A.* **2018**, *115*, 3563−3568.
(17) Khmelnitskiy, A.; Reinot, T.; Jankowiak, R. Mixed Upper Exciton State of the Special Pair in Bacterial Reaction Centers. *J. Phys. Chem. B* **2019**, *123*, 852−859.
(18) Arnett, D. C.; Moser, C. C.; Dutton, P. L.; Scherer, N. F. The First Events in Photosynthesis: Electronic Coupling and Energy Transfer Dynamics in the Photosynthetic Reaction Center from Rhodobacter sphaeroides. *J. Phys. Chem. B* **1999**, *103*, 2014−2032.
(19) Vos, M. H.; Breton, J.; Martin, J.-L. Electronic Energy Transfer within the Hexamer Cofactor System of Bacterial Reaction Centers. *J. Phys. Chem. B* **1997**, *101*, 9820−9832.
(20) Jankowiak, R.; Rancova, O.; Chen, J.; Kell, A.; Saer, R. G.; Beatty, J. T.; Abramavicius, D. Mutation-Induced Changes in the Protein Environment and Site Energies in the (M)L214G Mutant of the Rhodobacter sphaeroides Bacterial Reaction Center. *J. Phys. Chem. B* **2016**, *120*, 7859−7871.
(21) Haran, G.; Wynne, K.; Moser, C. C.; Dutton, P. L.; Hochstrasser, R. M. Level Mixing and Energy Redistribution in Bacterial Photosynthetic Reaction Centers. *J. Phys. Chem.* **1996**, *100*, 5562−5569.
(22) Fingerhut, B. P.; Mukamel, S. Resolving the Electron Transfer Kinetics in the Bacterial Reaction Center by Pulse Polarized 2-D Photon Echo Spectroscopy. *J. Phys. Chem. Lett.* **2012**, *3*, 1798−1805.
(23) Koepke, J.; Krammer, E.-M.; Klingen, A. R.; Sebban, P.; Ullmann, G. M.; Fritzsch, G. pH Modulates the Quinone Position in the Photosynthetic Reaction Center from Rhodobacter sphaeroides in the Neutral and Charge Separated States. *J. Mol. Biol.* **2007**, *371*, 396−409.
(24) Konig, C.; Neugebauer, J. Exciton Coupling Mechanisms Analyzed with Subsystem TDDFT: Direct vs Pseudo Exchange Effects. *J. Phys. Chem. B* **2013**, *117*, 3480−3487.
(25) Pavanello, M.; Van Voorhis, T.; Visscher, L.; Neugebauer, J. An accurate and linear-scaling method for calculating charge-transfer excitation energies and diabatic couplings. *J. Chem. Phys.* **2013**, *138*, 054101.
(26) Wesolowski, T. A.; Shedge, S.; Zhou, X. Frozen-Density Embedding Strategy for Multilevel Simulations of Electronic Structure. *Chem. Rev.* **2015**, *115*, 5891−5928 PMID: 25923542. .
(27) Casida, M. E.; Wesolowski, T. A. Generalization of the kohn-sham equations with constrained electron density formalism and its time-dependent response theory formulation. *Int. J. Quantum Chem.* **2004**, *96*, 577.
(28) Neugebauer, J.; Louwerse, M. J.; Baerends, E. J.; Wesolowski, T. A. The merits of the frozen-density embedding scheme to model solvatochromic shifts. *J. Chem. Phys.* **2005**, *122*, 094115.
(29) Konig, C.; Neugebauer, J. First-Principles Calculations of Electronic Spectra of Light-Harvesting Complex II. *Phys. Chem. Chem. Phys.* **2011**, *13*, 10475.
(30) Konig, C.; Schluter, N.; Neugebauer, J. Direct Determination of Exciton Couplings from Subsystem Time-Dependent Density-Functional Theory within the TammDancoff Approximation. *J. Chem. Phys.* **2013**, *138*, 034104.
(31) Bhandari, S.; Cheung, M.; Geva, E.; Kronik, L.; Dunietz, B. D. Fundamental gaps of condensed-phase organic semiconductors from single-molecule polarization-consistent optimally tuned screened range-separated hybrid functionals. *J. Chem. Theory Comput.* **2018**, *14*, 6287−6294.
(32) Bhandari, S.; Dunietz, B. D. Quantitative accuracy in calculating charge transfer state energies in solvated molecular dimers using screened range separated hybrid functional within a polarized continuum model. *J. Chem. Theory Comput.* **2019**, *15*, 4305.
(33) Song, Y.; Schubert, A.; Maret, E.; Burdick, R. K.; Dunietz, B. D.; Geva, E.; Ogilvie, J. P. Vibronic structure of photosynthetic pigments probed by polarized two-dimensional electronic spectroscopy and ab initio calculations. *Chem. Sci.* **2019**, *10*, 8143.
(34) Zheng, Z.; Egger, D. A.; Brédas, J.-L.; Kronik, L.; Coropceanu, V. Effect of solid-state polarization on charge-transfer excitations and transport levels at organic interfaces from a screened range-separated hybrid functional. *J. Phys. Chem. Lett.* **2017**, *8*, 3277−3283.
(35) Joo, B.; Han, H.; Kim, E.-G. Self-Sufficiency through Screened Exchange. *J. Chem. Theory Comput.* **2018**, *14*, 2823−2828.
(36) Caricato, M.; Mennucci, B.; Tomasi, J.; Ingrosso, F.; Cammi, R.; Corni, S.; Scalmani, G. Formation and relaxation of excited states in solution: A new time dependent polarizable continuum model based on time dependent density functional theory. *J. Chem. Phys.* **2006**, *124*, 124520.
(37) You, Z.-Q.; Mewes, J.-M.; Dreuw, A.; Herbert, J. M. Comparison of the Marcus and Pekar partitions in the context of non-equilibrium, polarizable-continuum solvation models. *J. Chem. Phys.* **2015**, *143*, 204104.
(38) Cammi, R.; Corni, S.; Mennucci, B.; Tomasi, J. Electronic excitation energies of molecules in solution: State specific and linear response methods for nonequilibrium continuum solvation models. *J. Chem. Phys.* **2005**, *122*, 104513.
(39) Shao, Y.; et al. Advances in methods and algorithms in a modern quantum chemistry program package. *Phys. Chem. Chem. Phys.* **2006**, *8*, 3172−3191.
(40) Reddy, N. R. S.; Kolaczkowski, S. V.; Small, G. J. Nonphotochemical hole burning of the reaction center of Rhodopseudomonas viridis. *J. Phys. Chem.* **1993**, *97*, 6934−6940.
(41) Breton, J. Orientation of the chromophores in the reaction center of Rhodopseudomonas viridis. Comparison of low-temperature linear dichroism spectra with a model derived from X-ray crystallography. *Biochim. Biophys. Acta, Bioenerg.* **1985**, *810*, 235−245.
(42) Neugebauer, J. Photophysical Properties of Natural Light-Harvesting Complexes Studied by Subsystem Density Functional Theory. *J. Phys. Chem. B* **2008**, *112*, 2207−2217.
(43) Schlau-Cohen, G. S.; De Re, E.; Cogdell, R. J.; Fleming, G. R. Determination of Excited-State Energies and Dynamics in the B Band of the Bacterial Reaction Center with 2D Electronic Spectroscopy. *J. Phys. Chem. Lett.* **2012**, *3*, 2487−2492.
(44) Konig, C.; Neugebauer, J. Quantum Chemical Description of Absorption Properties and ExcitedState Processes in Photosynthetic Systems. *ChemPhysChem* **2012**, *13*, 386−425.
(45) Ermler, U.; Fritzsch, G.; Buchanan, S. K.; Michel, H. Structure of the photosynthetic reaction centre from Rhodobacter sphaeroides at 2.65 A resolution: cofactors and protein-cofactor interactions. *Structure* **1994**, *2*, 925−936.
(46) Parson, W. W.; Warshel, A. In *The Purple Phototrophic Bacteria*; Hunter, C. N., Daldal, F., Thurnauer, M. C., Beatty, J. T., Eds.; Springer Netherlands: Dordrecht, 2009; pp 355−377.
(47) Parson, W.; Chu, Z.-T.; Warshel, A. Electrostatic control of charge separation in bacterial photosynthesis. *Biochim. Biophys. Acta, Bioenerg.* **1990**, *1017*, 251−272.
(48) Raszewski, G.; Diner, B. A.; Schlodder, E.; Renger, T. Spectroscopic Properties of Reaction Center Pigments in Photosystem II Core Complexes: Revision of the Multimer Model. *Biophys. J.* **2008**, *95*, 105−119.
(49) Romero, E.; Novoderezhkin, V. I.; van Grondelle, R. Quantum design of photosynthesis for bio-inspired solar-energy conversion. *Nature* **2017**, *543*, 355.
(50) Vacha, F.; Joseph, D. M.; Durrant, J. R.; Telfer, A.; Klug, D. R.; Barber, J. Photochemistry and spectroscopy of a five-chlorophyll reaction center of photosystem II isolated by using a Cu affinity column. *Proc. Natl. Acad. Sci. U. S. A.* **1995**, *92*, 2929−2933.
(51) Ohio Supercomputer Center; http://osc.edu/ark:/19495/f5s1ph73, 1987.

DOI: 10.1021/acs.jpcb.9b07646
J. Phys. Chem. B 2019, 123, 8970−8975